Structural, microstructural, and magnetic properties of nanocrystalline-amorphous Fe–Co–Ta–B alloy processed by high-energy mechanical alloying

Zohra Msetra, Nawel Khitouni, Abdulrahman Alsawi, Mohamed Khitouni, Virgil Optasanu, Joan-Josep Suñol, Mahmoud Chemingui

Journal Pre-proof

Structural, microstructural, and magnetic properties of nanocrystalline-amorphous Fe–Co–Ta–B alloy processed by high-energy mechanical alloying

Zohra Msetra, Nawel Khitouni, Abdulrahman Alsawi, Mohamed Khitouni, Virgil Optasanu, Joan-Josep Suñol, Mahmoud Chemingui

PII: S2238-7854(23)02309-8

DOI: https://doi.org/10.1016/j.jmrt.2023.09.183

Reference: JMRTEC 8590

To appear in: *Journal of Materials Research and Technology*

Received Date: 2 February 2023

Revised Date: 30 August 2023

Accepted Date: 18 September 2023

Please cite this article as: Msetra Z, Khitouni N, Alsawi A, Khitouni M, Optasanu V, Suñol J-J, Chemingui M, Structural, microstructural, and magnetic properties of nanocrystalline-amorphous Fe–Co–Ta–B alloy processed by high-energy mechanical alloying, *Journal of Materials Research and Technology*, https://doi.org/10.1016/j.jmrt.2023.09.183.

Structural, microstructural, and magnetic properties of nanocrystalline-amorphous Fe–Co–Ta–B alloy processed by high-energy mechanical alloying

Zohra Msetra[1], Nawel Khitouni[1], Abdulrahman Alsawi[2], Mohamed Khitouni[3*], Virgil Optasanu[4], Joan-Josep Suñol[5], Mahmoud Chemingui[1]

[1]Laboratoire de Chimie Inorganique, LR-11-ES-73, Faculté des Sciences de Sfax, Université de Sfax, BP 1171, Sfax 3018, Tunisia

[2]Department of Physics, College of Science, Qassim University, Buraidah 51452, Saudi Arabia

[3]Department of Chemistry, College of Science, Qassim University, Buraidah 51452, Saudi Arabia

[4]ICB, UMR 6303 CNRS, Université de Bourgogne Franche Comté, 9 av. Alain Savary, 21078 Dijon, France

[5]Department of Physics, University of Girona, Campus Montilivi, 17071 Girona, Spain

*Corresponding author. E-mail address: khitouni@yahoo.fr (M. Khitouni)

Abstract

A nanocrystalline Fe(Co) phase dispersed within an amorphous matrix was achieved after milling of $Fe_{31}Co_{31}B_{30}Ta_8$ powder mixtures up to 200 hours by using a high-energy ball mill. The transformations occurring in the powders during milling were studied with the use of X-ray diffraction and scanning electron microscopy techniques. The transformation of the phase depends upon the milling time. With the increase of milling time, various nanostructured phases such as Fe(Co), Co_2Ta, Co(Ta,B), fcc-Co, Fe- type borides, and amorphous phase were identified. Magnetic properties were also investigated and correlated with microstructural changes. By increasing milling time, irregular variation of saturation magnetization is identified in relation to the change in the composition of the system. Also, the gradual decrease in grain size to a few nanometers resulted in an increase in coercivity while increasing the milling time up to 200 hours. The existence of non-magnetic Ta and B atoms in the neighboring Fe and Co atoms and the increase in the volume fraction of the amorphous phase are retained as the major factors of this hard magnetic behavior of the present system.

Keywords: Mechanical alloying; Fe-Co-Ta-B system; Phase transitions; X-ray diffraction; Magnetic properties; Hard ferromagnetic behavior.

1. Introduction

Due to its potential uses in numerous technical fields, including electronics, ceramics, catalysis, structural components, and magnetic data storage, nanocrystalline/amorphous alloys have received a great deal of interest recently [1]. Due to their excellent soft magnetic characteristics, high mechanical strength, superior corrosion resistance, and focus on Co-based nanocrystalline /amorphous alloys in particular. These alloys are a highly attractive category of materials with unique characteristics. Additionally, they have the highest compressive yield strength measurements [2,3]. In addition, the magnetic behavior of co-based alloys is also remarkable due to their high permeability, good soft magnetic characteristics, zero magnetostriction, large magnetoimpedance, an exceptionally low coercive force, and excellent corrosion resistance [2]. Formation of suitable nanocrystalline/amorphous structure is usually achieved by optimization of alloy composition and technical processing. MA has attracted a lot of attention in recent years

because it has proved to be an ideal tool for the generation of a wide range of systems, including supersaturated solid solutions, dispersion-strengthened materials, intermetallic, nanocrystalline and amorphous materials, through complex mechanisms of intermixing, solid-state inter-diffusion and chemical reactions, depending on the various milling parameters [4,5,6]. In fact, during the MA process, the progressive increase in the density of lattice defects might influence the thermodynamics and kinetics of the mechanical reaction. It was reported by Park et al. [7,8] that the addition of an alloying element with positive heat of mixing with a constituent element in a given alloy system improves the amorphous formation ability and also the plasticity of the inherently brittle glassy alloy. Moreover, the addition of a certain amount of metalloids, in particular, B, Si, P, and C favors thermal stability and the soft magnetic behavior of alloys [9,10]. Moreover, the addition of small amounts of boron to alloys can modify the fracture mode from intergranular failure to transgranular fracture by being segregated to grain boundaries. Studies on the microstructure of these alloys gave evidence that the addition of boron can also result in the formation of Fe_2B precipitates and a tetragonal phase which is likely coherent with the matrix [11]. Boron has been also found to facilitate the development of amorphous and nanocrystalline structures [12, 13]. It has been reported that the addition of boron enhances the amorphization process after the segregation of B at grain boundaries [14,15]. Also, it results in an extension in the glass formation range and an improvement of soft magnetic properties [16,17]. Until today, some research has been carried out on the formation of amorphous in Co-Fe-B-Si-Ta melt-spun ribbons [18,19]. They reported that these ribbons showed an anomalous behavior in the temperature dependence of creep deformation, that is, the elongation by loading of the amorphous ribbons at high-temperature region was remarkably decreased by the addition of Ta, e.g. for $Fe_4Co_{74}Ta_4B_{18}$, in comparison with $Fe_4Co_{74}B_{22}$, and $Fe_4Co_{74}Si_4B_{18}$. This drastic change in high-temperature creep deformation due to the addition of Ta is considered to be related to some change in the packing fraction of the constituent elements. In fact, the existence of atomic pairs with large negative heat of mixing and sequential variations in the size of the constituents (B < Co < Fe < Ta) in the alloy, results in a high packing density of amorphous phase, and consequently its higher thermal stability [20]. Wu et al. [21] demonstrated the amorphization in a series of Co-Fe-(Ti-Zr)-B alloys with a large boron content of 3-30 at.%. The obtained amorphous powders exhibited a saturation magnetization in the ranges of 90-125 Am^2/kg, which is much larger than the magnetization range of rapidly-solidified Co-based glasses with a similar fraction of boron [22]. These prepared powders represented very large coercivities (4.8-8 kA/m), even after annealing treatment, indicating their poor soft magnetic properties [21]. Further investigations on glass formation in the Co-Fe-Ta-B and Co-Nb-Zr-B alloys with 30 at.% B revealed that in contrast to rapid solidification, the MA process is unable to produce a homogeneous glassy material even after a long milling period, which contributes to their inferior thermal stability and magnetic softness [3,23]. Avar et. al, developed mechanically alloyed $Co_{60}Fe_5Ni_5Ti_{25}B_5$ amorphous powders with a moderate saturation magnetization of 53.4 Am^2/kg and coercivity of 0.6 kA/m[24]. An amorphous $Co_{60}Fe_{18}Ta_8B_{14}$ powdered alloy was successfully prepared by Msetra et al. [13]. By the use of a high-energy mechanical alloying process above 50 h milling. This alloy exhibits a wide supercooled liquid region of 83 K and its crystallization occurs through three successive exothermic reactions. To the best of our knowledge, there is not much research focused on the study of the relationship between microstructural properties and physical properties in mechanically alloyed CoFeTaB alloys. In this work, we report a new nanocrystalline-amorphous $Co_{31}Fe_{31}B_{30}Ta_8$ alloy prepared by high-energy mechanical alloying. We

explore the synergistic effect of increasing the alloying time on the refinement in the microstructure and its effects on magnetic properties.

2. Materials and Methods

Elemental powders (99.9% purity, from Alpha Aesar) of Co, Fe, Ta, and B of the nominal composition $Fe_{31}Co_{31}B_{30}Ta_8$ powders were MA by using a planetary ball-mill (Type Retsch PM200) under Ar atmosphere (99.999 purity). The ball-to-powder weight ratio used was maintained at 8:1, and the milling speed was adjusted to 350 rpm. The milling was performed with hardened stainless-steel balls and vials, with seven balls (10 mm diameter), and to prevent excessive heating, the mill was subjected to cycles (10 min on, 5 min off). X-ray diffraction measurements (XRD) were performed using Siemens D-500 equipment with CuK_α radiation. The microstructural characteristics and chemical compositions were extracted from the refinement of XRD patterns using the Rietveld-based MAUD program [24]. Throughout the procedure, the diffraction profiles are simulated using analytical functions. To match the data profiles and estimate the lattice strain and average crystallite size from the isotropic model, a pseudo-Voigt analytical function was used. The morphology of MA powders was examined by scanning electron microscopy (SEM) in a DSM960A ZEISS microscope with eenergy-dispersiveX-ray microanalysis (EDS). The magnetic parameters of the powders milled, namely saturation magnetization (Ms), the remanence (Mr), the coercivity (Hc), and the squareness ratio (Mr/Ms), were measured using a Quantum Design SQUID MPMS-XL superconducting quantum interference device at 5 K in a maximum field of 50 kOe.

3. Results and discussion

3.1. SEM analysis

Micrographs of the powder mixture of $Co_{31}Fe_{31}B_{30}Ta_8$ produced both before and after mechanical alloying are shown in Figure 1. At first (before milling), one can distinguish two families of particles: Spherical and rod or irregular-shaped particles (Fig.1a) correspond, respectively, to the elements Co, Fe, and Ta. After 5 h of milling, heterogeneity in particle size and shape is clearly shown (Fig. 1b). Following high-intensity mechanical alloying shocks, both the welding and fracture of some particles can be seen. As the milling period increases to 75 hours (Fig. 1c), intense shear and impact forces are applied to the particles, causing them to break into smaller powders with irregular morphologies and wide size variations. The size of the powder particles and the irregularity of their shapes tend to decrease with more milling, and the size distribution narrows, as seen in Fig. 1d. Additionally, the morphology of the powder particles becomes more uniform. The powder particles get finer by extending the MA process to 200 hours, probably as a result of the continued development of the amorphous phase in their structural makeup (Fig. 1e). In fact, as milling time increases, the alloy hardens more quickly due to a strong plastic deformation effect. The powder particles become more brittle as a result of this hardening, increasing the rate at which they fracture. After a specific amount of milling time, the size of the particles in some systems does not vary, suggesting that the rates of fragmentation and agglomeration have reached equilibrium [25]. Figure 1f displays the EDS analysis and mapping of the powder that was obtained after 200 hours of milling. Co, Fe, and Ta were present in the initial mixture, according to the EDS analysis. However, the EDS mapping reveals that the powders become inhomogeneous, and distinct clusters of Fe and Co indicate the development of the FeCo phase towards the end result of the powder mixture's milling. Despite being produced in

an argon atmosphere, a small amount of oxidation (oxygen presence in yellow color) was observed. The powders may show this low oxygen content after they have been milled and taken for analysis. The atomic concentration of the elements Fe, Co, Ta, and B is 33:29:7:31 These values are slightly different from those of the nominal composition: 31:31:30:8. In fact, the iron content is higher than that used before the milling process which may be due to iron contamination from the jars and balls. Moreover, the lack of contents of the Co and Ta can be attributed to the sticking of the particles of the powders to the walls of the jars and to the surface of the balls.

Figure 1

3.2. X-ray analysis

Figure 2 displays the $Co_{31}Fe_{31}B_{30}Ta_8$ powders' X-ray patterns as a function of milling time. Pre-milling patterns reveal the existence of all principal X-ray peaks corresponding to the initial constituent elements: hcp-Co (space group P63/mmc; a=2,500 Å and c= 4.140 Å), c.c-Fe (space group Im-3m; a=2.866 Å), cubic-Ta (space group Im-3m, a=3.306 Å) and rhombohedral-B (space group R-3m, a=8.740 Å and c=5.030 Å). When this superposition of patterns is observed qualitatively, it can be seen that during milling, certain peaks vanish and others appear, suggesting possible phase transitions carried on by the mechanical alloying. Additionally, during the milling process, a small shift of the major diffraction peak on either side of its initial position was seen. This shift can be explained by changes in the lattice parameter or by changes in the distribution of the atoms Co, Fe, B, and Ta as a result of the milling process, which results in the formation of new solid solutions. Moreover, the shift of peaks can probably be caused by the lattice expansion due to the increase in the density of dislocations with their characteristic strain fields on the nanograin boundary. The Co changes from its hcp to fcc form allotropically after 5 hours of milling. This phenomenon can be attributed to the existence of stacking defects produced by plastic deformation during the MA [29]. In a subsequent study, this phase transition was detected following 2h of milling under identical mechanosynthesis protocols [13]. Also, the Rietveld refinement reveals the phases hcp-Co (a = 2.513(1); c = 4.078(1)Å), fcc-Co (a = 3.532(1) Å), Fe (a = 2.877(1) Å), and B (a = 8.623(1); c = 5.112(1) Å), as well as new metastable bcc-FeCo phase (a = 2.8575 Å) and $Fe_{23}B_6$ and low content of cubic-Co_2Ta (a = 6.533 (1)). The production of the metastable fcc-$Fe_{23}B_6$ type boride after 5 h of milling may be related to the significant number of structural flaws that increase the atomic diffusivity of boron. Additionally, the alloying element Ta might make it easier to create the metastable $Fe_{23}B_6$ phase, which has relatively high free energy. On the other hand, Fe dissolves more readily in the Co lattice than Ta does, according to the literature. Therefore, a significant quantity of elastic energy is needed for Ta to dissolve in the Co lattice. As a result, Ta dissolves more slowly than Fe does, requiring longer milling times [25,30]. This explains why, after 5 hours of milling, the Ta has a low content.

Figure 2

After 15 hours, it is possible to see a decrease in the peak's intensity that corresponds to the Ta crystalline structure as well as the disappearance of some peaks that correspond to the structure of hcp-Co. The cubic-Co_2Ta phase (a = 6.653(1) Å) is continuously formed as a result of this evolution. Additionally, the production of the Fe_3B-type boride phase (a=5.4165(1); c=4.3616(1) Å) can be seen after 15h of milling.

According to the reaction $Fe_{23}B_6 \rightarrow 5Fe + 6Fe_3B$ [31,32], this phase appears to be created by the transformation of the boride type $Fe_{23}B_6$ (which occurs after 5 hours of milling). After 30 hours of milling, the peaks corresponding to the Ta structure completely vanish, and the boron atoms in the interstitial sites dissolve [33], which causes the network to compress at the level of the occupied sites and ultimately leads to the formation of the supersaturated solid solution of Co(Ta, B) (a=10.423(1)Å). The intense plastic deformation and increased energy storage provided by mechanical alloying thereby facilitate this phase transition. The mechanical alloying process then stores a large number of the material's flaws [30]. At the same time, the best Rietveld refinement identifies a tetragonal-Fe_2B (a=5.254(1); c=4.276(1)Å) phase. After 75 h of milling, all identified nanocrystalline are superimposed to a broad halo typical of a highly disordered amorphous phase with an amount of 25 %. Indeed, it has been demonstrated that adding B to the $Co_{60}Fe_{18}B_{14}Ta_8$ composition, which is thought to be an amorphized element [34], enhances the production of an amorphous phase for a considerable amount of milling time [35]. However, continued milling for up to 200 hours causes the recrystallization of nanocrystalline Fe(Co) (a=2.8651(1)Å; wt%=60%), which was refined with a significant amount around 40 % of an amorphous phase (see Fig. 3).

Figure 3

In general, the impact of plastic deformation produced during milling and supersaturated solid solutions formed during the dissolution of the Co, Ta, and B elements can be connected to the change in crystal characteristics. In fact, the existence of these flaws will disrupt the vacancy-surrounded lattices' structure, which will eventually result in a deformed crystalline lattice. When the crystallites are larger than a few nanometers, this can become more intense [36]. The distribution of the initial element is responsible for the apparent irregularity in the evolution of the lattice parameter characteristics as a function of milling time. In addition, the boron particles' action on the iron matrix and/or the development of metastable solid solutions, which is why the density of defects increased during milling, may have caused the lattice to vary, increasing or decreasing lattice parameters [37]. On the other hand, it is important to note that the competition between the amount of lattice strains produced by a milling device and the high degree of dynamic recovery in the milled material can be used to explain the characteristics of the nanocrystalline structure; in other words, this structure was created by the evolution from a dislocation cell structure with dislocation cells and low angle boundaries to a nearly uniform random structure made up of nanocrystals with high angle boundaries. As a result, the variation of the average of the crystallite size, D, and the lattice strain rate, (ε), of the $Co_{31}Fe_{31}B_{30}Ta_8$ powder as a function of milling time is shown in Figure 4. The evolution of the two microstructural characteristics appears to be competitive. The MA compound exhibits a steady decrease in crystallite size, which is compatible with the milling effect, according to a comparative analysis of crystallite size evolution. It is evident that during the initial milling stage (0–50 h), the size of the crystallites rapidly reduces until it reaches values of the order of 30 nm at 75 h of milling. This is caused by the process of internal energy growth, which leads to ongoing grain refinement. The main reason why the size of the crystallites decreases during milling by crystallite fracturing may be the steady rise in dislocation density that leads to hardening. After 200 hours, the crystallite size value attained is in the range of 9 nm. Figure 5 also shows the lattice strains of the alloy powder as they change over time in relation to milling time. We observe a significant increase during the initial milling stages (0–50h) before reaching a stage of stabilization at prolonged times. 1.2% is the final measured size value

of lattice strain. In most cases, large dislocation densities and an increase in grain boundary fraction can cause lattice strain increase [38]. In actuality, when the powder particles are refined, the grains get more and more filled with crystalline flaws. Additionally, because the influence of atomic size is less noticeable in an amorphous phase than in a crystalline lattice, an amorphization can be seen during milling by an extreme rise in crystalline defects and more so those of the grain boundaries [39]. When the proportion of the amorphous phase is around 45 % (see Fig. 8), this can result in saturation with the evolution of the rate of lattice strains after 165 hours of milling.

Figure 4

3.3. Magnetic study

The hysteresis loops of the $Co_{31}Fe_{31}B_{30}Ta_8$ samples, which were recorded at 300 K, are shown to depend on milling time in Figure 5. The milled powders display the same ferromagnetic behavior with sigmoidal hysteresis curves as those that are typically seen in nanostructured materials with small magnetic domains [40]. With the independence of the Fe-based solid solution concentrations as identified by XRD investigation, the magnetic characteristics continue to be only partially stable. Similar results have been discovered in earlier investigations [41,42]. Thus, the development of the FeCoTaB phases does not significantly alter magnetic behavior; rather, the local environment of the Fe atoms and their interatomic distance will have the greatest impact. It is also well known that the magnetic characteristics of materials strongly depend on their magnetostriction, magnetic anisotropy, particle shape anisotropy, internal stress, and microstructure evolution [43]. The greatest difference observed is found in the milled sample for 135 hours which has its saturation much higher than any other milled sample (Fig. 5). Moreover, when milling time varies, it can be seen that cycles flatten. This might be a result of the alloys' extremely high anisotropy constant value.

Figure 5

The microstructural evolution that the samples underwent as a result of the mechanical alloying procedure can be responsible for the changes in the magnetic characteristics. Fig. 6 presents both the variation of the coercivity, Hc, and the inverse of grain size as a function of milling time. Various phenomena, such as soft ($Hc<1000$ A/m), hard ($Hc>1000$ A/m) [44], and superparamagnetic ($Hc\sim0$ A/m) [45] behaviors, have been advantageously designed with the support of nanocrystalline ferromagnetic materials. In the present study, the Hc ranges from 7800 to 35240 A/m, resulting in the material being mechanically alloyed and becoming a hard ferromagnetic material. The variation of the coercivity, Hc, during the milling process, can be described as a gradual increase depending on milling time. During the milling process, the refinement of grain size and the introduction of various structural flaws can both affect coercivity behavior. Thus, the fact that the grain sizes are greater than the domain wall thickness and that the grain boundaries act as barriers to domain wall motion can contribute to the rise in coercivity. In fact, the random anisotropy model [46] states that Hc obeys a 1/D-dependence law when the ferromagnetic exchange length, Lex, is greater than or equal to the grain size, D. and the inverse grain size and as a function of milling time. As shown by the plot of the coercivity vs inverse grain size for the same sample (see the inset in Fig. 6) the coercivity is universally found inversely proportional to the grain size. However, the coercivity determined by grain boundaries can be expressed as [47]:

$$Hc \sim 3 \frac{\gamma_\omega}{Ms} \frac{1}{D}$$

where γ_ω is the wall energy, and Ms is the saturation magnetization. The wall energy $\gamma_\omega$can be estimated by the equation:

$$\gamma_\omega \sim \sqrt[3]{\frac{k_B T_c K_1}{a}}$$

thus

$$Hc \sim \sqrt[3]{\frac{k_B T_c K_1}{aMs}} \frac{1}{D}$$

where $k_B$is the Boltzmann constant, K_1 is the magneto-crystalline anisotropy, T_c is the Curie temperature, and a is the lattice constant.

On the other hand, the increase in coercivity Hc can be explained as the result of a significant introduction of high internal stresses into the material, which is intimately connected to the process [48,49]. Thus, the effect dominating the coercivity by way of the magnetoelastic interaction has been characterized as magnetostriction in combination with the high internal strain [50]. On the other hand, the slight decrease of Hc between 30 and 40 h of milling can be related to the reduction of hcp-Co volume fraction (hcp-Co transforms to fcc-Co and fcc Co-based phases) since, in general, hcp structures are known to have larger magnetocrystalline anisotropy than fcc ones [51]. The formation of boride-type phases, Fe3B and Fe2B, at the grain boundaries and the fragmentation of magnetic particles during the milling process may also be factors in this decrease in Hc. These processes result in a heterogeneous ferromagnetic system where the Fe-rich and Co-rich ferromagnetic grains are separated by Ta and/or B elements.

Figure 6

The variations in saturation magnetization (Ms) with milling time offered lighter on the mechanisms involved in mechanical alloying. The curve (M-H), which corresponds to the atomic structure of magnetism, can be used to calculate this magnetic property. As a result, it may be described using the metal's chemical composition, electronic structure, and magnetic exchange between its dipoles. However, the local environment of the atoms and the quantum phenomena present have a significant impact on each of these metal's characteristics [52]. Additionally, the Ms was calculated by applying the following classical law of approach to saturation [53]:

$$M = Ms\left(1 - \frac{a}{H} - \frac{b}{H^2}\right) - \chi H$$

where H is the applied field, χ is the field-independent susceptibility, and a and b are coefficients that depend on the magnetic and structural properties of the sample [41,60]. With the assumption of a random exchange interaction and the application of a field high enough to completely saturate the sample, the following semi-empirical relationship is produced [54,55]:

$$A = \alpha(4\rho\pi Ms)P_{eff}$$

where α is a constant that is usually around 0.1, ρ is the density of the material, and P_{eff} is the effective fraction of porosity and non-magnetic inclusions [54,56].

The change in the values of Ms in Fe31Co31Ta8B30 mixed powders as a function of milling duration is depicted in Figure 7. As can be seen, the magnetization rises to 163

emu/g after 2 hours of milling before falling to 99 emu/g after 45 hours. When compared to powders that were received, this decrease can be attributed to the effects of lower particle size and D. However, as milling is continued to 135 h, the Ms rises to its highest value of 133 emu/g. Since each grain may now be thought of as a single magnetic domain, eliminating the impact of the magnetic walls, this rise may be attributed to domain wall motion (spin rotation), which results in a reduction in magneto-crystalline anisotropy [57–59]. Additionally, the progressive development of the FeCo phase, which reaches its highest proportion after 135 hours of milling, can be used to explain the significant increase in Ms approaching its maximum value. According to reports, FeCo alloys have the highest Ms of any alloy (~235 emu/g) [60]. At 200 hours of the milling process, the Ms parameter had dropped to 110 emu/g. The recovery of ferromagnetism produced by Fe sites, which may be related to the disordering of the alloy during milling, is responsible for the apparent drop in Ms [61]. Additionally, the electrons introduced by the addition of Ta and B atoms during milling, which are paramagnetic and non-magnetic, respectively, can be linked to the decreases in Ms through changes in 3d band structure (ferromagnetic interaction between Fe-Fe sites).

Figure. 7

The remanence-to-saturation ratio, Mr/Ms is an important magnetic parameter in determining the magnetic energy. The Mr/Ms ratio's variation as a function of milling time is shown in Figure 7. Due to the fact that both the Mr/Ms and the Hc parameters are structurally sensitive, their tendency during processing time is almost identical. Accordingly, the Mr/Ms ratio variations are mostly the result of processing conditions, and their explanation is related to the microstructural change that the metallic system undergoes during mechanical alloying. As shown in Figure 7, the ratio Mr/Ms increases as a function of milling time, that is to say when grain size decreases. The obtained final ratio value of about 0.21 after 200 hours of milling indicates that small magnetic particles are typically single domains. In general, the ratio (Mr/Ms) measures how squared the hysteresis loop (M-H) is and is connected to the intensity of inter-grain interactions. According to the Stoner-Wolfarth model, the reduced remanence in single-domain particles with uniaxial anisotropy is of the order of Mr/Ms = 0.5 [61].

Additional information about the processes taking place during mechanical alloying is provided by the variation in saturation magnetization (Ms) with milling time and system composition. Figure 8 displays both the variation of the saturation magnetization, Ms, and the system composition as a function of milling time. After 5 hours of milling, Ms decreases with increasing milling time, reaches a value of about 100 $emu.g^{-1}$ after 45 h, and then, it increases again until it reaches a value of 134 $emu.g^{-1}$ after 75 h. The decrease of Ms indicates a significant change in the magnetic moment due to the existence of non-magnetic Ta and B atoms in the neighboring Fe and Co atoms. The new increase, after 45 h of milling, can be explained by the rise in the amounts of Fe- and Co-based supersaturated solid solutions. It is worth noting that the value of Ms obtained at 75 hours of milling (134 $emu.g^{-1}$) is shown lower than that obtained after 5 hours (163 $emu.g^{-1}$) because in the case of the pure phases Fe and Co the magnetization at saturation is higher than that of the phases contaminated by Ta and B markedly. In addition, Ms reaches a peak value at 135 hours of milling, and then it decreases to an average value of 110 $emu.g^{-1}$ at the end of milling due to the increase of amorphous phase volume fraction. Indeed, if the grain sizes are small enough, the structural distortions associated with the surfaces/interfaces reduce the magnitude of the saturation magnetization owing to the deviation of interatomic spacings in the interfacial regions.

Figure. 8

4. Conclusion

In summary, a nanocrystalline Fe(Co) phase dispersed within an amorphous matrix (around 62%) is achieved after milling of Fe, Co, Ta, and B powder mixtures up to 200 hours; First, the microstructural and magnetic properties were studied as a function of the milling time, and secondly, we tried to look into the dependence of the magnetic properties on the microstructure obtained during the milling process. The formation of various phases as well as Fe(Co), Co2Ta, Co(Ta, B), fcc-Co, Fe- borides nanocrystals, and amorphous phase was followed by XRD patterns as a function of milling times up to 200 hours. At the end of milling, a nanostructure of Fe(Co) dispersed within an amorphous matrix (56%) is achieved after 200 hours of milling. From the perspective of magnetism, there is a correlation between microstructural evolution and magnetic behavior, whereby a reduction in crystallite size to a few nanometers results in an increase in the coercivity and squareness ratio, which increases magnetism. Therefore, a harder, ferromagnetic material is produced as the crystallite size decreases. Further, an irregular variation of the saturation magnetization was recorded as a function of milling time. This magnetic behavior was interpreted by the dependence of magnetization on the chemical composition of the system obtained during mechanical milling. Indeed, the existence of non-magnetic Ta and B atoms in the neighboring of Fe and Co atoms and the increase of amorphous phase volume fraction cause a significant change in the magnetization. The coercivity, Hc, and magnetization saturation, Ms, values specific to the final product of the milling process are about 35000 A/m and 110 emu.g−1, respectively.

5. References

[1] Krasnowski M, Kulik TJ. Nanocrystalline FeAl intermetallic produced by mechanical alloying followed by hot-pressing consolidation. Intermetallics 2007;15: 201.

[2] Inoue A, Shen BL, Koshiba H, Kato H, Yavari AR. Ultra-high strength above 5000 MPa and soft magnetic properties of Co–Fe–Ta–B bulk glassy alloys. Acta Mater. 2004;52: 1631.

[3] Taghvaei AH, Stoica M, Khoshkhoo MS, Thomas J, Vaughan G, Janghorban K, Eckert J. Microstructure and magnetic properties of amorphous/nanocrystalline Co40Fe22Ta8B30 alloy produced by mechanical alloying. Mater. Chemi. Phys. 2012; 134: 1214.

[4] Suryanarayana C. Mechanical Alloying and Milling. Prog. Mater. Sci. 2001; 1: 46.

[5] Bormio-Nunes C, Dias MB, Ghivelder L. High magnetostriction of the polycrystalline alloy (Fe0. 8Al0. 2) 97B3. Journal of Alloys and Compounds 2003; 574: 467–471.

[6] Han Y, Kong FL, Han FF, Inoue A, Zhu SL, Shalaan E, Al-Marzouki F. New Fe-based soft magnetic amorphous alloys with high saturation magnetization and good corrosion resistance for dust core application Intermetallics 2016; 76: 18-25.

[7] Park ES, Kim DH, Ohkubo T, Hono K. Enhancement of glass forming ability and plasticity by addition of Nb in Cu–Ti–Zr–Ni–Si bulk metallic glasses. Non Cryst. Solids., 2005; 351: 1232.

[8] Park ES, Kim DH. Phase separation and enhancement of plasticity in Cu–Zr–Al–Y bulk metallic glasses. Acta Mater., 2006; 54: 2597.

[9] Lu Z, Li H, Lei Z, Chang C, Wang X, Lu Z. The effects of metalloid elements on the nanocrystallization behavior and soft magnetic properties of FeCBSiPCu amorphous alloys. Metals. 2018; 8: 283

[10] Khitouni N, Daly R, Escoda L, Llorca-Isern N, Suñol JJ, Dammak M, Khitouni M. The Effect of B and Si Additions on the Structural and Magnetic Behavior of Fe-Co-Ni Alloy Prepared by High-energy Mechanical Milling. Journal of Superconductivity and Novel Magnetism, 2020; 33: 2727–2735.

[11] Pang L, Kumar KS. Effect of heat treatment on the microstructure of an Fe-40Al-0.7 C-0.5 B alloy. Mater. Sci. Eng. A. 1998 ; 258 :161–166.
[12] Kane SN, Gupta A, Gercsi Z, Mazaleyrat F, Varga, LK. Mössbauer and magnetic studies of (Fe100− xCox) 62 Nb8B30 (X= 0, 33, 50) alloys. Magn. Magn. Mater. 2005; 292: 447
[13] Msetra Z, Khitouni N, Suñol JJ, Khitouni M, Chemingui M. Characterization and thermal analysis of new amorphous Co60Fe18Ta8B14 alloy produced by mechanical alloying. Materials Letters 2021; 292: 129532.
[14] Hasegawa R, Ray R. Iron-boron metallic glasses. J. Appl. Phys., 1978; 49 : 4174.
[15] Gomez-Polo C. Magnetic properties of Fe-based soft magnetic nanocrystalline alloys. Magn. Mater. J., 2008; 320: 1984.
[16] Ohnuma S, Nose M, Shirakawa K, Masumoto T. Magnetic properties of amorphous Fe-Zr-B alloys. Sci. Rep. Res. Inst. Tohoku Univ., 1981; 29: 254.
[17] Inoue A, Kobayashi K, Nose M, Masumoto T. Mechanical properties of (Fe, Co, Ni)-MB (M= Ti, Zr, Hf, V, Nb, Ta and Mo) amorphous alloys with low boron concentration. J Phys. C., 1980; 41: 831.
[18] Ishlkawa, W, Hayashi K, Matsuda H, Hayakawa M, Ochiai Y, Aso K. Density of CoFeTaB amorphous alloys. Acta Metallurgica 1988; 36(4): 811-816.
[19] Jiyun Oh, Haein Choi-Yim, Ki Hoon Kang. Thermal and magnetic properties of the Co-Fe-B-Si-Ta alloy system for several Fe/Co ratios. Journal of the Korean Physical Society 2016; 69: 1813–1816.
[20] Taghvaei AH, Khoshrodi AM. Characterization, thermodynamic analysis, and magnetic investigation of new soft magnetic amorphous/nanocrystalline Co50Fe21Ti19Ta5B5 powders produced by mechanical alloying, J. Alloys Comp. 2018; 742: 887.
[21] Wu HM, Hu CJ, Li HC. Formation of Co–Fe–M–B (M= Zr, Ti) amorphous powders by mechanical alloying and their magnetic properties, Journal of Alloys and Compounds, 2009; 483: 553-556.
[22] Itoi T, Inoue A. Thermal stability and soft magnetic properties of Co–Fe–M–B (M= Nb, Zr) amorphous alloys with the large supercooled liquid region, Materials Transactions, JIM, 2000; 41: 1256-1262.
[23] Moreno L, Blázquez J, Ipus J, Conde A. Amorphization and evolution of magnetic properties during mechanical alloying of Co 62 Nb 6 Zr 2 B 30: Dependence on starting boron microstructure, Journal of Alloys and Compounds, 2014; 585: 485-490.
[24] Lutterotti L, Bortolotti M, Ischia G, Lonardelli I., Wenk HR. "Rietveld texture analysis from diffraction images, Z. Kristallogr., Suppl. 2007; 26: 125-130.
[25] Jaffari Jezeh MR, Tavoosi M, Ghasemi A, Farshadnia R. Metastable phases in Co70B20Si5Fe4Mo1 alloy fabricated by non-equilibrium processes, Non-Crystalline.Solids. 2015; 427: 26–33.
[26] Mohamed F. A., “A dislocation model for the minimum grain size obtainable by milling,” Acta Materialia, 2003; 51(14): 4107–4119.
[27] Fecht H.-J., “Nanostructure formation by mechanical attrition,” Nanostructured Materials, 1995; 6:(1-4); 33–42.
[28] Rawers J. and Cook D., Influence of attrition milling on nano-grain boundaries. Nanostructured Materials, 1999; 11(3): 331–342.
[29] Sort J, Nogues J, Surinach S, Munoz JS, Baro MD. Correlation between stacking fault formation, allotropic phase transformations and magnetic properties of ball-milled cobalt. Mater. Sci. Eng. 2004; 869A: 375–377.
[30] Taghvaei AH, Stoica M, Vaughan G, Ghaffari M, Maleksaeedi S, Janghorban K. Microstructural characterization and amorphous phase formation in

Co40Fe22Ta8B30 powders produced by mechanical alloying, J. Alloys Compd. 2012; 512: 85–93.
[31] Raanaei H, Fakhraee M. Synthesis and characterization of nanocrystalline Co-Fe-Nb-Ta-B alloy, Magnetism and Magnetic Materials 2017; 438: 144–15.
[32] Shokrollahi H. The magnetic and structural properties of the most important alloys of iron produced by mechanical alloying, Materials and Design 2009; 30: 3374–3387.
[33] Börner L, Eckert J. Nanostructure formation and steady-state grain size of ball-milled iron powders, Mater. Sci. Eng. 1997; A226/228: 541-545.
[34] Pilar M, Escoda L, Suñol JJ, Greneche JM. Magnetic study and thermal analysis of a metastable Fe-Zr based alloy: Influence of process control agents. J. Magn. Magn. Mater.2008; 320: 823–827.
[35] Sunol JJ, Pradell T, Clavaguera N, Claveguera-Mora MT. Mössbauer spectroscopy Study of the Crystallisation Behaviour of Fe-Ni-Si-P amorphous powders prepared by Ball Milling. Journal of Metastable and Nanocrystalline Materials 2001; 10: 525-530.
[36] Krifa M, Mhadhbi M, Escoda L, Güell JM, Sunol JJ, Llorca-Isern N, Artieda- Guzmán C, Khitouni M. Phase transformations during mechanical alloying of Fe–30%Al–20% Cu, Powder Technology, 2013; 246: 117-124.
[37] Chater R, Bououdina M, Chaanbi D, Abbas H. Synthesis and magnetization studies of nanopowder Fe70Ni20Cr10 alloys prepared by high energy milling. Solid State Chemistry 2013; 201: 317–323.
[38] Hamzaoui R, Cherigui M, Guessasma S, Elkedimand O, Fenineche N. Artificial neural network methodology: Application to predict magnetic properties of nanocrystalline alloys. Materials Sci. Engi. A, 2009; 163: 17-21.
[39] Schaffer GB, McCormick PG, Mechanical alloying. Mater. Forum 1992; 16: 91-97.
[40] Nowroozi MA, Shokrollahi H. The effects of milling time and heat treatment on the micro-structural and magnetic behavior of Fe42Ni28Zr8Ta2B10C10 synthesized by mechanical alloying. J. Magn. Magn. Mater. 2013; 335: 53–58.
[41] Krifa M, Mhadhbi M, Escoda, L, Güell JM, Sunol JJ, Llorca-Isern, N, Artieda-Guzmán C, Khitouni M. Nanocrystalline (Fe60Al40)80Cu20 alloy prepared by mechanical alloying. Journal of Alloys and Compounds 2013; 554: 51-58.
[42] Ibn Gharsallah H, Sehri A, Aabou M, Escoda L, Sunol JJ, Khitouni M. Structural and Thermal Study of Nanocrystalline Fe-Al-B Alloy Prepared by Mechanical Alloying. Metall. Mater. Trans. A 2015; 46: 3696–3704.
[43] Sharifati A, Sharafi S. Structural and magnetic properties of nanostructured (Fe70Co30)100−xCux alloy prepared by high energy ball milling. Mater. Des. 2012; 41: 8–15.
[44] Coey JMD. Magnetic materials. J. Alloys Compd. 2001; 326: 2–6.
[45] Degauque J. Magnétisme et matériaux magnétiques : introduction. J. Phys. IV 2, 1992 ; C3.1–C3: 13.
[46] Herzer G. Grain size dependence of coercivity and permeability in nanocrystalline ferromagnets. IEEE Trans. Magn. 1990; 26(5): 1397-1402.
[47] Yu RH, Basu S, Zhang RY, Parvizi-Marjidi A, Unruh KM, Xiao JQ. High-temperature soft magnetic materials: FeCo alloys and composites. IEEE Trans Magn 2000; 36(5):3388–93.
[48] Hamzaoui R, Elkedim O, Gaffet E. Milling conditions effect on structure and magnetic properties of mechanically alloyed Fe–10% Ni and Fe–20% Ni alloys. Mater. Sci. Eng. A, 2004; 381: 363–371.
[49] Gras C, Gaffet E, Bernard F. Niepce JC. Enhancement of self-sustaining reaction by mechanical activation: case of an Fe+2Si system. Sci. Eng. A 1999; 264: 94–107.

[50] Herzer G. Soft magnetic nanocrystalline materials. Scripta Metall. Mater. 1995; 33: 1741–1756.
[51] Weller D, Harp GR, Farrow RFC, Cebollada A, Sticht J. Orientation dependence of the polar Kerr effect in fcc and hcp Co. Phys. Rev. Lett. 1994; 72: 2097.
[52] Karimi L., and Shokrollahi H., Structural, microstructural and magnetic properties of amorphous/nanocrystalline Ni63Fe13Mo 4Nb20 powders prepared by mechanical alloying. J.Alloys.Compd., 2011, 509, 6571-6577.

[53] Chikazumi S., in: Physics of magnetism, Wiley, New York, 1964, p 277.

[54] Zeng Q., and Baker I., Magnetic properties and thermal ordering of mechanically alloyed Fe–40 at% Al. Intermetallics., 2006; 14: 396-405.

[55] Schlomann E., Properties of Magnetic Materials with a Nonuniform Saturation Magnetization. I. General theory and calculation of the static magnetization. J. Appl. Phys.,1967; 38: 5027-5034.

[56] Dionne G.F., Weiss J.A., and Gary A.A., Hysteresis loops modeled from coercivity, anisotropy, and microstructure parameters. J. Appl. Phys., 1987; 61: 3862-3864.
[57] Bhoi B., Srinivas V., and Singh V., Evolution of microstructure and magnetic properties of nanocrystalline Fe70-xCuxCo30 alloy prepared by mechanical alloying. J. Alloys Compd.,2010; 496: 423-428.

[58] Sharifati A., and Sharafi S., Structural and magnetic properties of nanostructured (Fe70Co30)100-xCux alloy prepared by high-energy ball milling. Mater. Des., 2012; 41: 8-15.

[59] Kalita M.P.C., Perumal A., and Srinivasan A., Structure and magnetic properties of nanocrystalline Fe75Si25 powders prepared by mechanical alloying. Magn. Magn. Mater.,2008; 320: 2780-2783.

[60] A. Zelenakova, D. Oleksakova, J. Degmova J. Kovac, P. Kollar, M. Kusy, P. Sovak, Structural and ´ magnetic properties of mechanically alloyed FeCo powders. Journal of Magnetism and Magnetic Materials, 316 (2) (2007) 519–522.

[61] Hernando A, Gonzalez JM. Soft and hard nanostructured magnetic materials. Hyperfine Interactions. 2000; 130: 221-240.

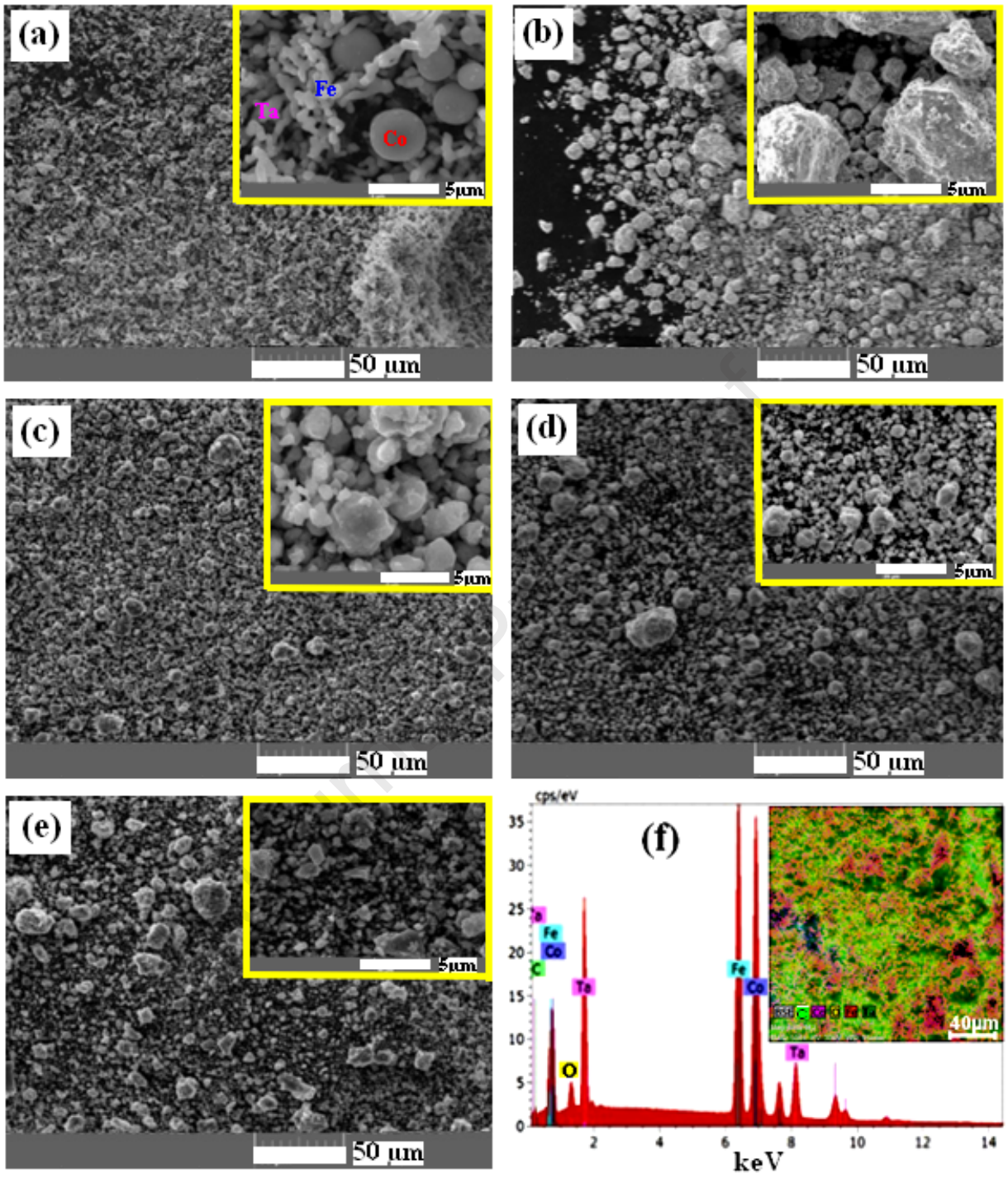
(a)
Fe
Ta
Co
5μm
50 μm
(b)
5μm
50 μm
(c)
5μm
50 μm
(d)
5μm
50 μm
(e)
5μm
50 μm
(f)
cps/eV
Fe
Co
C
Ta
O
Fe
Co
Ta
40μm
keV

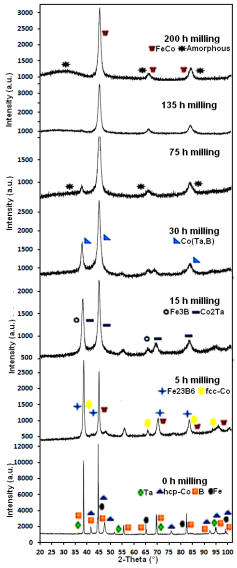

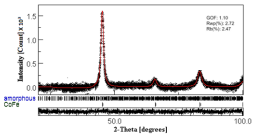

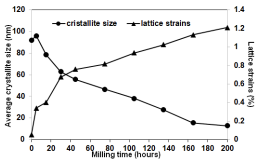

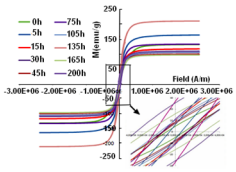

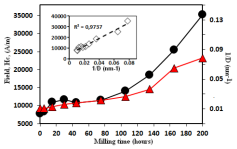

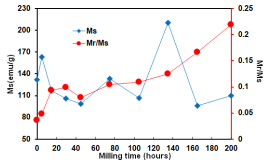

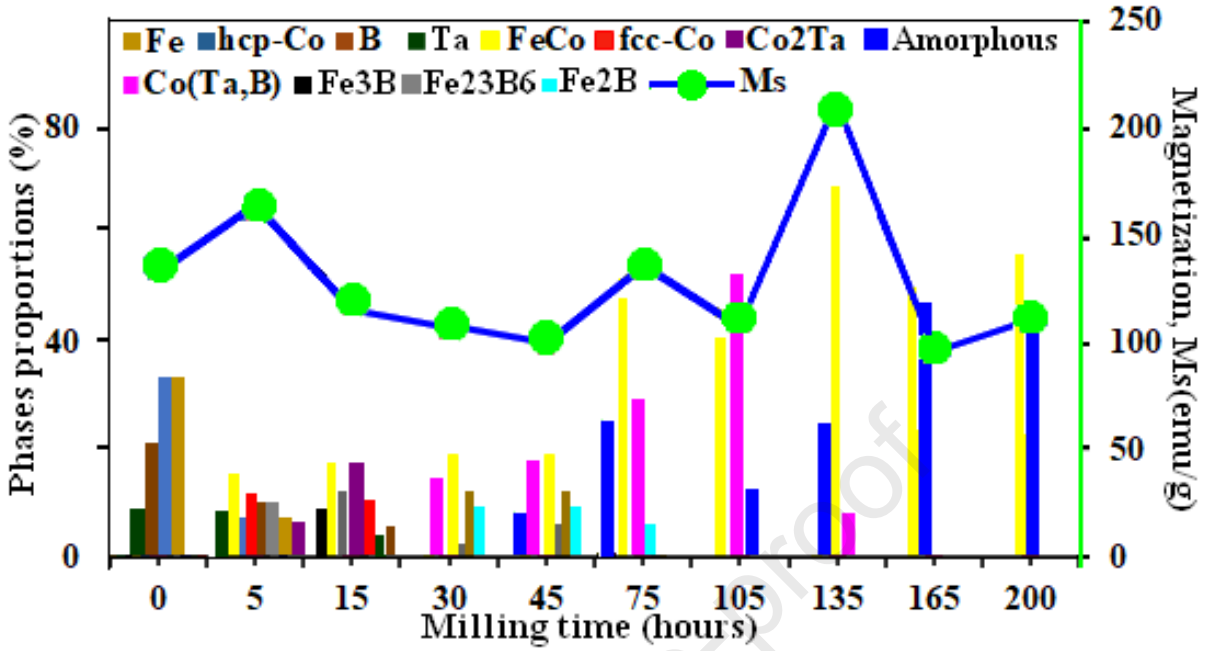

Declaration of interests

☒ The authors declare that they have no known competing financial interests or personal relationships that could have appeared to influence the work reported in this paper.

☐ The authors declare the following financial interests/personal relationships which may be considered as potential competing interests: